

Optimization of Coverage and Capacity Using Smart Antennae

Min-Che Ho, Pin-Yu Song, Yi-Shian Chiou *, Yueh-Tan Lee and Li-Ling Huang

Department of Civil Engineering, National Central University, Tao-Yuan 320317, Taiwan; b1231520002000@gmail.com (M.-C.H.); parn.feng@msa.hinet.net (P.-Y.S.); 10007950@mail.tycg.gov.tw (Y.-T.L.); irenahf@gmail.com (L.-L.H.)

* Correspondence: lettermail64@gmail.com; Tel.: +886-955075859

Abstract: In the rural and geographically remote regions of Taiwan, the high cost of establishing information infrastructure has resulted in significantly lower internet penetration and usage rates compared with urban areas. To address the network demands in such remote mountainous areas, the deployment of multiple mobile base stations has become essential. However, the wireless implementation of base stations can lead to signal interference issues. This research aims to enhance the signal reception capabilities of end-user devices by utilizing intelligent directional antennas. This study employs five directional smart antennas, each of which can be independently adjusted to be active or inactive. Unlike traditional omnidirectional antennas that cause interference in overlapping coverage areas for end-user devices, our proposed adaptive directional antenna algorithm optimizes energy consumption by selectively activating directional antennas and concurrently reduces signal interference problems for end-user devices. The results of this research offer valuable insights for improving network connectivity and efficiency in remote and underserved areas. Through experimental simulations conducted in an environment with 10 base stations per square kilometer, the utilization of smart antennas, as opposed to omnidirectional antennas, results in a significant improvement of 33.8% in signal coverage.

Keywords: coverage and capacity optimization; smart antennae; power control



Citation: Ho, M.-C.; Song, P.-Y.; Chiou, Y.-S.; Lee, Y.-T.; Huang, L.-L. Optimization of Coverage and Capacity Using Smart Antennae. *Appl. Sci.* **2023**, *13*, 10897. <https://doi.org/10.3390/app131910897>

Academic Editor: Christos Bouras

Received: 23 July 2023

Revised: 8 September 2023

Accepted: 25 September 2023

Published: 30 September 2023



Copyright: © 2023 by the authors. Licensee MDPI, Basel, Switzerland. This article is an open access article distributed under the terms and conditions of the Creative Commons Attribution (CC BY) license (<https://creativecommons.org/licenses/by/4.0/>).

1. Introduction

Traditional base stations rely on wired backhaul network technologies, such as fiber optics, Digital Subscriber Line (xDSL), and Hybrid Fibre-coax, as the backend communication solutions. Among these options, fiber optic communication networks have become the primary choice for fixed-point base station backhaul transmission. However, the deployment of fiber optic networks entails lengthy pre-installation procedures, requiring approval from local authorities for road excavation or shared pipeline usage. Moreover, access to the interior of buildings necessitates consent from the property owners, adding to the cost and time required for fiber optic network implementation due to administrative constraints. As a result, the construction and scheduling of fiber optic networks often face challenges and complexities, impeding infrastructure development.

To address these issues, wireless loop solutions have been increasingly discussed and proposed, leveraging the characteristics of wireless networks to reduce the need for civil engineering during network deployment. By doing so, not only can the costs of construction be lowered, but also the speed of base station equipment installation can be increased. In particular, for communication infrastructure requirements in the mountainous areas of Taiwan, a wireless backhaul network presents an excellent option, as it eliminates the need for physically laying cables, facilitating the provision of wireless internet services to remote regions while ensuring uninterrupted connectivity, even in the face of natural disasters. Additionally, the same infrastructure can serve as a vital relay point for activities such as landslide monitoring, forest fire detection, and environmental monitoring.

In recent years, artificial intelligence methods have been applied in various fields to solve practical problems. In particular, issues such as network resource allocation and base station configuration, which belong to the realm of mathematical optimization theory, can be addressed using deep learning methods [1,2]. The integration of Internet of Things (IoT) technologies plays a significant role in various applications, relying heavily on signal coverage rates and data transmission rates in network communications [3–6]. Therefore, this paper aims to investigate the maximization of base station coverage in wireless backhaul networks. Signal interference remains a primary concern for base stations, encompassing two main scenarios: inter-cell interference from large-scale base stations [7] and co-channel interference between micro base stations [8,9]. These interferences can lead to adverse effects on user network quality, causing delays, disconnections, and signal loss.

To address the first scenario, the 3rd Generation Partnership Project (3GPP) introduced Enhanced Inter-Cell Interference Coordination (eICIC) to reduce interference between macro and small cells by implementing the Almost Blank Sub-frames (ABS) mechanism. However, the issue of mutual interference between base stations has not yet reached a unified standard approach. Currently, the most common method to control wireless signal interference between base stations is adjusting the transmission power of the base stations. Numerous studies have proposed algorithms to mitigate inter-cell interference, with the ICIC [10] and Coverage and Capacity Optimization (CCO) [11] solutions from 3GPP release 8 being the most representative ones. Furthermore, due to the limited spectrum resources, some researchers have developed frequency reuse methods to allow the reuse of the same frequency bands. This is because when adjacent base stations transmit using the same frequency, it can lead to interference. In situations with limited bandwidth, allocating the optimal frequency bands to base stations helps mitigate interference among them [12]. However, traditional inter-cell interference coordination mainly focuses on coordinating interferences between macro base stations and resolving edge interference problems. With the integration of heterogeneous networks, interferences are no longer confined to macro base stations, especially in the ever-changing environments where micro base stations operate. Owing to their ease of installation by ordinary users without professional on-site testing, micro base stations face much more complex interference environments than traditional macro base stations. As a result, the probability of user device disconnection and retransmission significantly increases due to environmental interference and changes in transmission channels. In this study, we explore this issue and propose potential solutions.

This paper seeks to utilize intelligent antenna technology, allowing base stations to adapt their antenna radiation patterns and power to reduce the probability of user interference or disconnection when entering high-interference areas.

2. Small-Cell Interference

In a traditional omni-directional antenna base station network environment, when user equipment (UE) is located within the overlapping coverage areas of two base stations, as shown in Figure 1, it will receive transmission signals from both Base Station 1 (BS1) and Base Station 2 (BS2). This situation leads to signal interference issues for UE1, as it receives signals from both BS1 and BS2 while being within the coverage range of both base stations. The same applies to UE2.

One approach to address this type of interference is illustrated in Figure 2. By adjusting the transmission power of the traditional omni-directional antenna, the transmission power of BS2 can be reduced. As a result, the overlapping coverage area between BS1 and BS2 will be decreased, effectively resolving the interference problems experienced by UE1 and UE2.

Reducing the power of the base station can effectively shrink the overlapping coverage area between base stations, resolving interference issues for user equipment (UE), as illustrated in Figure 3a. Prior to adjusting the transmission power of Base Station 2 (BS2), all UEs, including UE1, UE2, . . . , and UE6, were within the coverage areas of both Base Station 1 (BS1) and BS2, resulting in a 100% overall network coverage rate. However, due to the interference between UE1 and UE2, lowering the transmission power of BS2

(as shown in Figure 3b) effectively resolved the interference problem for UE1 and UE2. Nevertheless, this action also led to a decrease in the coverage rate, as UE5 was no longer within the coverage range of BS2 and, thus, could not receive signals. Consequently, the overall network coverage rate dropped to 83%.

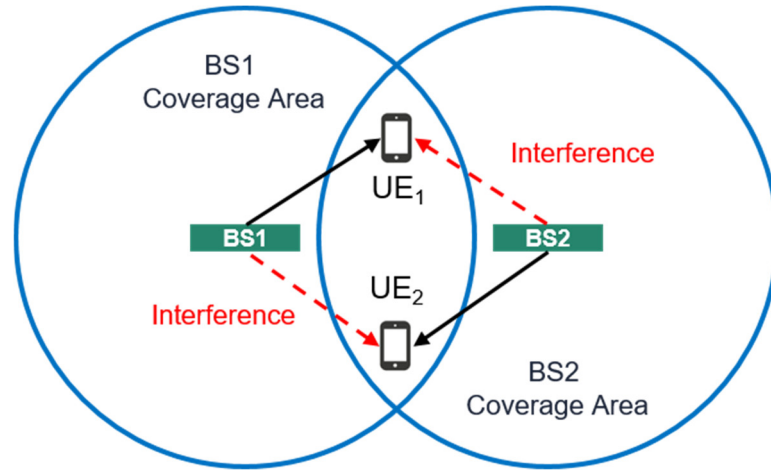


Figure 1. Interference caused to terminals by traditional omnidirectional antennae.

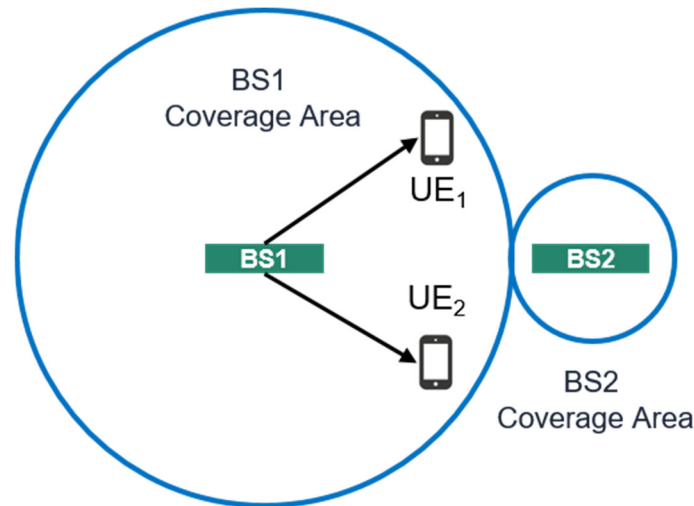
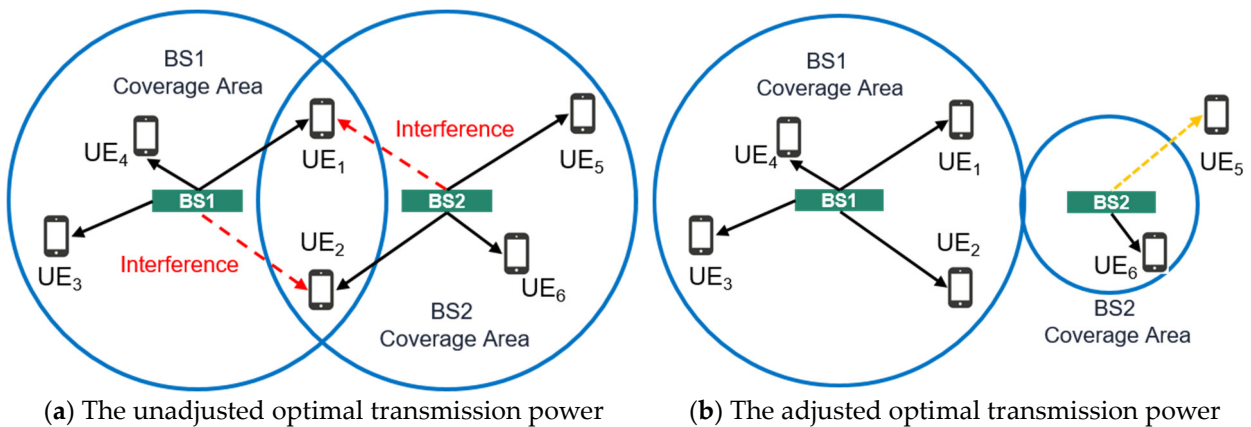


Figure 2. Adjusting the power of omnidirectional antennae to reduce interference.



(a) The unadjusted optimal transmission power

(b) The adjusted optimal transmission power

Figure 3. Adjusting the power reduces interference, but reduces UE coverage.

Many scholars have proposed innovative smart antenna designs based on antenna theory. These designs enable signals to be utilized more effectively during both reception and transmission, thereby achieving communication or sensing objectives [13,14]. In order to simultaneously maintain a high base station coverage rate and effectively reduce UE interference issues, this study employed intelligent adaptive directional antennas for the base stations. Unlike traditional omni-directional antennas, where the antenna gain remained the same at different angles, intelligent adaptive directional antennas can control the signal strength in different directions, resulting in varying antenna gains for terminal devices at different angles. Figure 4 represents the intelligent adaptive directional antenna used in this study. The antenna with only a degree zero sector was activated. This represents the radiation pattern of the base station's transmitted signal. Taking the degree zero direction as an example, it is evident from the diagram that the emission intensity in the degree zero direction was greater than in the other directions.

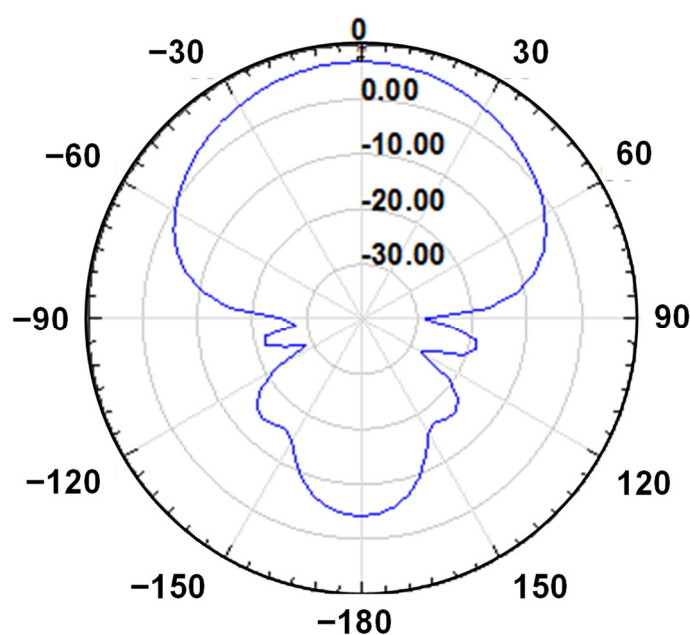


Figure 4. Smart directional antenna.

Figure 5 illustrates the solution using intelligent adaptive directional antennas. In Figure 5a, the traditional omni-directional antenna architecture shows that UE1, UE2, . . . , and UE6 were all within the coverage areas of BS1 and BS2, resulting in an overall network coverage rate of 100%. However, interference issues occurred between UE1 and UE2. By adopting the intelligent adaptive directional antenna architecture shown in Figure 5b, the transmission power of BS1 and BS2 could be adjusted along with the directional antennas. This not only resolved the interference problem for UE1 and UE2, but also maintained the overall network coverage rate at 100%.

Each directional antenna can be adjusted to be on or off, enabling various radiation patterns. In this study, there were five antenna directions, each of which could be activated or deactivated. This allowed for a total of $2^5 = 32$ possibilities. Assuming there were N base stations in the entire network system, each base station had M levels of adjustable power and C antenna directions. The total number of possibilities was then $(M \times C)^N$. The research objective of this study was to determine the power level and the combination of antenna directions (on or off) for each base station throughout the network system in a way that simultaneously achieved a high network coverage rate and reduced UE signal interference issues.

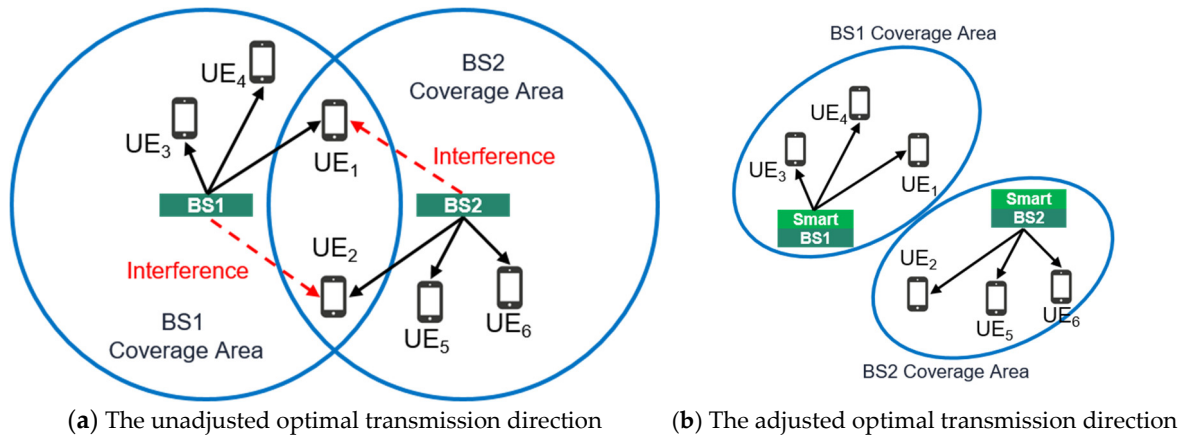


Figure 5. Smart directional antennae reduce interference while maintaining coverage.

3. Methodology

3.1. Modeling

Assuming the entire network system consists of n base stations, denoted as, S_i for $i = 1, 2, \dots, n$, each base station has j antenna directions. Let X_j^i represent the j -th antenna direction for the i -th base station. If $X_j^i = 1$, the antenna in that direction is activated, and if $X_j^i = 0$, the antenna is deactivated. Each base station has a maximum power of P_{max} and a minimum power of P_{min} . Additionally, each S_i can provide a bandwidth of up to B and can simultaneously serve a maximum of t_{S_i} terminal devices.

In the entire system, there are K terminal devices, denoted as u_1, u_2, \dots, u_k , with B_k representing the bandwidth that u_k can be allocated. P_i represents the power of S_i , PL denotes the path loss signal attenuation, γ represents the path loss exponent (where $\gamma \geq 2$), and d_{k,S_i} indicates the distance between u_k and base station S_i . A detailed explanation of the system model parameters is shown in Table 1.

Table 1. System parameter settings.

S_i	$S_i (i= 1, 2, \dots, n)$ Denote n Small Cells
X_j^i	The antenna beam j ($j = 1, 2, \dots, m$) of small cell S_i
R_j^i	The coverage area that user k can be served by S_i under the smart antenna X_j^i
P_{max}	Maximum transmission power of each small cell
P_{min}	Minimum transmission power of each small cell
B	Bandwidth of the channel
t_{S_i}	Number of users covered by S_i
B_k	$B_k = \frac{B}{t_{S_i}}$, the bandwidth that user k can use
K	Number of total users
p_i	The transmission power of small cell S_i
PL	Path loss
d_{k,S_i}	The distance between user k and small cell S_i
γ	Path loss exponent ($\gamma \geq 2$)

3.2. Coverage Model

The calculation of the coverage rate for traditional omni-directional antennas involves determining the radius within which the base station can transmit at its maximum power. The area of the circle with this radius is then calculated to represent the coverage area. However, for intelligent adaptive directional antennas, the coverage area varies depending

on which antenna directions are activated or deactivated. Therefore, the coverage rate [15] calculation in this study is represented by Formula (1), as follows:

$$\text{Coverage rate} = \frac{1}{K} \sum_{k=1}^K u_k \tag{1}$$

$$u_k = \begin{cases} 1, & \text{user } k \text{ under the coverage area } R_j^i \\ 0, & \text{otherwise} \end{cases}$$

where u_k equals 1 if u_k is within the coverage range (denoted as R_j^i) of the antenna in the direction where $X_j^i = 1$ for S_i . We can use the signal-to-interference-plus-noise ratio $SINR_k \geq \theta$ of u_k to determine whether it is covered by S_i . The coverage rate is calculated as follows: (number of UE serviced by the base station/number of UE unable to connect to the base station) * 100%.

3.3. Capacity Model

The calculation of network capacity is based on the Shannon Capacity [16] Formula (2), where B represents the system bandwidth, received power denotes the power received by u_k , and noise power represents the power of other interference noise

$$\text{Shannon capacity} = B \cdot \log_2 \left(1 + \frac{\text{received power}}{\text{noise power}} \right) \tag{2}$$

In the system model in this study, the capacity for each u_k is given by Formula (3), as follows:

$$B_k \cdot \log_2 \left(1 + \frac{p_i - \left[PL(d_1) + 10 \cdot \log_{10} \left(\frac{d_{k, S_i}}{d_1} \right)^\gamma \right]}{\sum_{h \neq i} \left\{ p_h - \left[PL(d_1) + 10 \cdot \log_{10} \left(\frac{d_{k, S_h}}{d_1} \right)^\gamma \right] \right\} + \sigma} \right) \tag{3}$$

where p_i is the transmission power of S_i , B_k is the bandwidth allocated to u_k , $PL(d_1)$ represents the signal attenuation value when u_k is 1 m away from S_i , and $PL(d_{k, S_i}) = PL(d_1) + 10 \cdot \log_{10} \left(\frac{d_{k, S_i}}{d_1} \right)^\gamma$ represents the signal attenuation value when u_k is d_{k, S_i} meters away from S_i . p_h represents the transmission power of S_h when $h \neq i$, and σ is the Gaussian noise, which considers the interference caused by base stations other than S_i to u_k .

Formula (3) calculates the capacity for one u_k . To calculate the overall network system capacity, considering there are K u_k in total, after implementing intelligent adaptive directional antennas, we know that u_k is within the coverage range of the j -th antenna ($X_j^i = 1$) for S_i and can benefit from an additional signal gain represented by G_j^i . Therefore, we can derive the overall network system capacity shown in Formula (4) based on Formula (3), as follows:

$$\sum_{k=1}^K B_k \cdot \left\{ u_k \cdot \log_2 \left(1 + \frac{p_i - \left[PL(d_1) + 10 \cdot \log_{10} \left(\frac{d_{k, S_i}}{d_1} \right)^\gamma \right] + \left(X_j^i \cdot G_j^i \right)}{\sum_{h \neq i} \left\{ p_h - \left[PL(d_1) + 10 \cdot \log_{10} \left(\frac{d_{k, S_h}}{d_1} \right)^\gamma \right] \right\} + \sigma} \right) \right\} \tag{4}$$

3.4. Objective Function

Based on Sections 3.2 and 3.3, we can define the objective function, denoted as $f(P, X)$, in this study shown in Formula (5) as follows:

$$f(P, X) = Cov \cdot \sum_{k=1}^K u_k + Cap \cdot \sum_{k=1}^K B_k \cdot \left\{ u_k \cdot \log_2 \left(1 + \frac{p_i - \left[PL(d_1) + 10 \cdot \log_{10} \left(\frac{d_k, S_i}{d_1} \right)^\gamma \right] + (X_j^i \cdot G_j^i)}{\sum_{h \neq i} \left\{ p_h - \left[PL(d_1) + 10 \cdot \log_{10} \left(\frac{d_k, S_h}{d_1} \right)^\gamma \right] \right\} + \sigma} \right) \right\} \tag{5}$$

$$P = \{p_i\}, i = 1, 2, \dots, n$$

$$X = \{X_j^i\}, i = 1, 2, \dots, n; j = 1, 2, \dots, m$$

where $P = \{p_i\}; i = 1, 2, \dots, n$ represents the transmission power of each base station; and $S_1, S_2, \dots, S_n, X = \{X_j^i\}; i = 1, 2, \dots, n$, and $j = 1, 2, \dots, m$ represent the antenna in the j -th direction of the base station S_i . If the antenna is activated, $X_j^i = 1$; otherwise, $X_j^i = 0$. Cov and Cap are normalized factors.

The trade-off between coverage and capacity is a well-recognized issue. When optimizing for coverage, it is challenging to achieve the specified transmission efficiency or capacity. Conversely, when optimizing for capacity, resources are prioritized for users very close to the base station, resulting in a decrease in coverage. Solutions to this multi-objective optimization problem have been proposed in research [17]. Our objective is to find a set of P and X that can maintain a high network coverage rate while reducing UE interference issues. By optimizing the objective function $f(P, X)$, the goal is to achieve an efficient combination of transmission power settings and antenna configurations to enhance overall network performance, which is subject to the following factors:

1. $P_{min} \leq p_i \leq P_{max}$
2. $SINR_k \geq \theta, \forall k = 1, 2, \dots, K, \text{ if } u_k = 1,$

$$\text{where } SINR_k = \frac{p_i - [PL(d_1) + 10 \cdot \log_{10} \left(\frac{d_k, S_i}{d_1} \right)^\gamma] + (X_j^i \cdot G_j^i)}{\sum_{h \neq i} \left\{ p_h - [PL(d_1) + 10 \cdot \log_{10} \left(\frac{d_k, S_h}{d_1} \right)^\gamma] \right\} + \sigma}$$

3. Each small cell can serve, at most, t users
4. There are t_{S_i} users covered by S_i
5. $B_k = \frac{B}{t_{S_i}}$
6. $\gamma \geq 2$
7. $u_k = \begin{cases} 1, & \text{user } k \text{ under the coverage area } R_j^i \\ 0, & \text{otherwise} \end{cases}$
8. $X_j^i = \begin{cases} 1, & \text{Antenna beam } j \text{ turns on the small cell } S_i \\ 0, & \text{otherwise} \end{cases}$
9. $R_j^i = \begin{cases} 1, & \text{if } X_j^i = 1 \\ 0, & \text{otherwise} \end{cases}$

3.5. Algorithms

The calculation mechanism for adjusting the on and off functions of the intelligent directional antenna of the base station and for determining the transmission power value can now be presented as Algorithms 1 and 2, as follows:

Algorithm 1 Find user's servingcell

```

1.  threshold = T
2.  Ncell = 10
3.  Nuser = 1000
4.  Nsector = 5
5.  CM = InitCell(Ncell)
6.  UM = InitUser(Nuser)
7.
8.  for u ∈ UM do
9.    for c ∈ CM do
10.     SNR = getSnr(c,u)
11.     if SNR ≥ threshold then
12.       R = getRegion(c,u)
13.       R.add(u)
14.     end if
15.   end for
16. end for
17.
18. for epoch = 1 to (Ncell * Nsector) do
19.   (C',R') = find Max User(CM)
20.   for u ∈ R' do
21.     u.servingcell = C'
22.     for c ∈ CM do
23.       if u is under the region R of c && c ≠ C' then
24.         R.remove(u)
25.       end if
26.     end for
27.   end for
28. end for

```

Algorithm 2 Decrease each cell's power

```

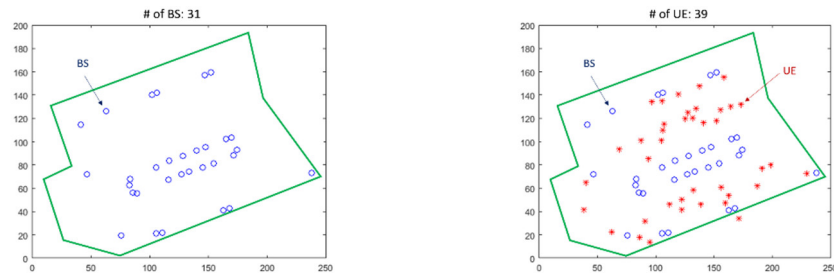
1.  threshold = T
2.
3.  for c ∈ CM do
4.    flag = True
5.    while c.isNotM inPower() && flag == True do
6.      c.powerDown(1)
7.      for each user u which is under the service of c do
8.        SNRlater = getSnr(c,u)
9.        if SNRlater < threshold then
10.         c.powerUp(1)
11.         flag = False
12.         break
13.       end if
14.     end for
15.   end while
16. end for

```

4. Evaluation

4.1. Experimental Setup

This research conducted experiments in the parking lot of National Central University, Taiwan, as shown in Figure 6. The area of the parking lot is 250 m by 200 m. The experiment involved 31 base stations (BS) and 39 user equipment (UE) items distributed in the parking lot, as illustrated in Figure 6a,b, respectively.



(a) The distribution of base stations' locations (b) The distribution of users' locations

Figure 6. Taiwan National Central University.

The experimental parameters were set as shown in Table 2. The experiment involved placing $K = 39$ signal receivers to simulate users within the NCU parking lot, and conducting trials with $n = 31$ base stations. Each base station comprised $j = 5$ directional antennas. Based on current commercial base station capabilities, the transmission power ranged from -19 dBm to 30 dBm, with an average data transmission rate of 20 Megabits per second.

Table 2. Parameter settings for simulation.

Area	250 m × 200 m
n	31
j	5
P_{max}	19 dBm
P_{min}	-30 dBm
B	20 Mbps
K	39
γ	2

The antenna configurations (X_j^i) for each direction of S_i and the number of covered UEs are listed in Table 3. This study conducted a small-scale algorithm verification within the experimental environment of the NCU parking lot. For broader areas and a larger user base, experiments were simulated to demonstrate the feasibility of extending the research methodology to other remote mountainous regions.

Table 3. On/off status of antenna X_j^i in the j th direction of S_i .

S_i	$X_j^i=1, \text{ Antenna on}; X_j^i=0, \text{ Antenna off}$					Covered Users
	X_1^i	X_2^i	X_3^i	X_4^i	X_5^i	
S_1	0	0	0	0	0	0
S_2	0	0	0	0	0	0
S_3	0	0	1	1	0	4
S_4	0	1	0	0	0	4
S_5	0	1	0	1	0	2
S_6	0	0	0	0	0	0

Table 3. Cont.

S_i	$X_j^i=1, \text{ Antenna on}; X_j^i=0, \text{ Antenna off}$					Covered Users
	X_1^i	X_2^i	X_3^i	X_4^i	X_5^i	
S_7	1	0	0	0	1	5
S_8	0	0	0	0	0	0
S_9	0	0	0	0	1	1
S_{10}	0	0	0	0	0	0
S_{11}	0	0	0	0	0	0
S_{12}	0	0	0	0	0	0
S_{13}	0	0	0	0	1	3
S_{14}	0	0	0	0	1	1
S_{15}	0	0	0	0	0	0
S_{16}	0	0	1	0	0	1
S_{17}	0	0	0	0	0	0
S_{18}	0	0	0	0	0	0
S_{19}	0	0	0	0	0	0
S_{20}	0	0	1	0	0	5
S_{21}	0	0	0	0	0	0
S_{22}	0	0	0	0	0	0
S_{23}	0	1	1	0	0	3
S_{24}	0	0	0	0	0	0
S_{25}	0	0	1	1	0	2
S_{26}	0	1	0	1	0	3
S_{27}	0	0	0	0	0	0
S_{28}	0	0	0	0	0	0
S_{29}	0	1	0	0	0	1
S_{30}	0	0	0	0	1	3
S_{31}	0	0	0	1	0	1
	Total UEs					39

4.2. Different Numbers of UEs

This research conducted experiments in a test area with dimensions of 1000 m by 1000 m. The number of base stations (BS) was fixed at 10, while the number of user equipment (UE) items varied from 200, 400, 600, 800, and 1000 to 1200. The experimental parameters were set as shown in Table 4.

Table 4. Parameter settings for different numbers of UEs case.

Area	1000 m × 1000 m
n	10
j	5
P_{max}	19 dBm
P_{min}	−30 dBm
B	20 Mbps
K	200–1200
γ	2

The results of the experiments are presented in Figure 7, which shows that the coverage rate ranged from 50% to 80%. This variation in coverage rate was due to the random distribution of UEs in the test area. Compared with omnidirectional antennas, when the number of users was 200, the majority of users could be covered adequately using omnidirectional antennas due to the lower user count. However, as the user count increased to 1200, simulation results indicated that the proposed approach enhanced coverage by approximately 23.6%. The CCO algorithm for smart antennas proposed in this study effectively enhanced the coverage rate of base stations.

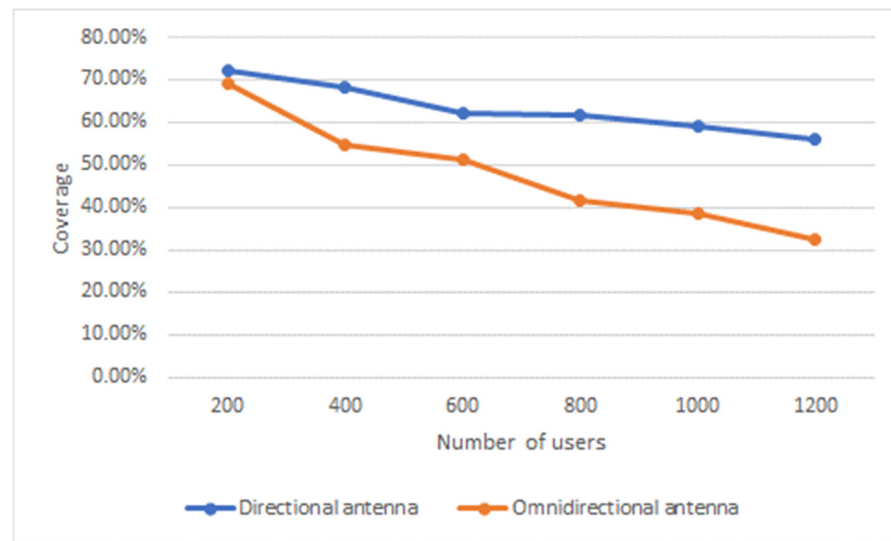


Figure 7. Experimental results (1000 m × 1000 m, no. of BSs = 10).

4.3. Different Numbers of BSs

The test area remained at 1000 m by 1000 m, with a fixed number of 1000 user equipment (UE) items. However, the number of base stations (BSs) was varied, including 2, 4, 6, 8, 10, and 12. The experimental parameters were set as shown in Table 5.

Table 5. Parameter settings for different numbers of BSs case.

Area	1000 m × 1000 m
n	2~12
j	5
P_{max}	19 dBm
P_{min}	−30 dBm
B	20 Mbps
K	1000
γ	2

The results of the experiments are presented in Figure 8, which shows that the coverage rate increased as the number of BSs increased. This was because, with a higher number of BS, there were more base stations available to provide service to the UEs. As a result, UE items had a higher chance of being served by at least one of the base stations, leading to an improvement in the overall coverage rate. Taking the number of base stations into consideration, when the base station count increased to 12, utilizing omnidirectional antennas covered only 38.3% of the service area. However, employing smart antennas enhanced the signal coverage rate to 78.1%. This approach effectively adjusted the radiation pattern of the base stations, transmitting signals in the direction of users, thereby substantially improving the signal coverage rate.

4.4. Field Sizes

The test area was adjusted to different dimensions, including 100 m by 100 m, 200 m by 200 m, 400 m by 400 m, 600 m by 600 m, 800 m by 800 m, and 1000 m by 1000 m. The number of user equipment (UE) items was fixed at 1000, and the number of base stations (BSs) remained at 10. The experimental parameters were set as shown in Table 6.

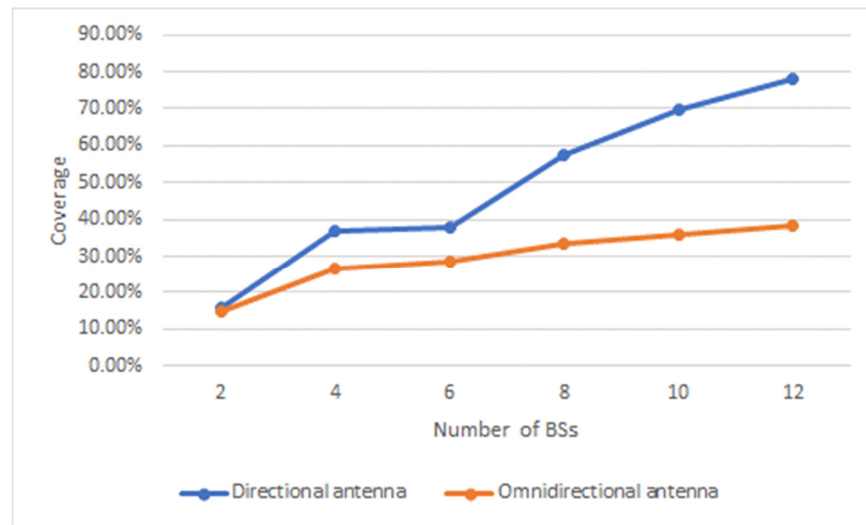


Figure 8. Experimental results (1000 m × 1000 m, no. of UEs = 1000).

Table 6. Parameter settings for field sizes case.

Area	100 m × 100 m–1000 m × 1000 m
n	10
j	5
P_{max}	19 dBm
P_{min}	−30 dBm
B	20 Mbps
K	1000
γ	2

The results of the experiments are presented in Figure 9, indicating that the coverage rate decreased as the test area increased. This is because, with a larger test area and a fixed number of base stations, the number of base stations available to serve each UE remained the same. As a result, the probability of UEs being served by a base station decreased, leading to a reduction in the overall coverage rate as the test area expanded. The simulation results demonstrated that, in larger testing areas, such as 1000 square meters, compared with conventional omnidirectional antennas, this method could enhance the field coverage rate by 42.8%.

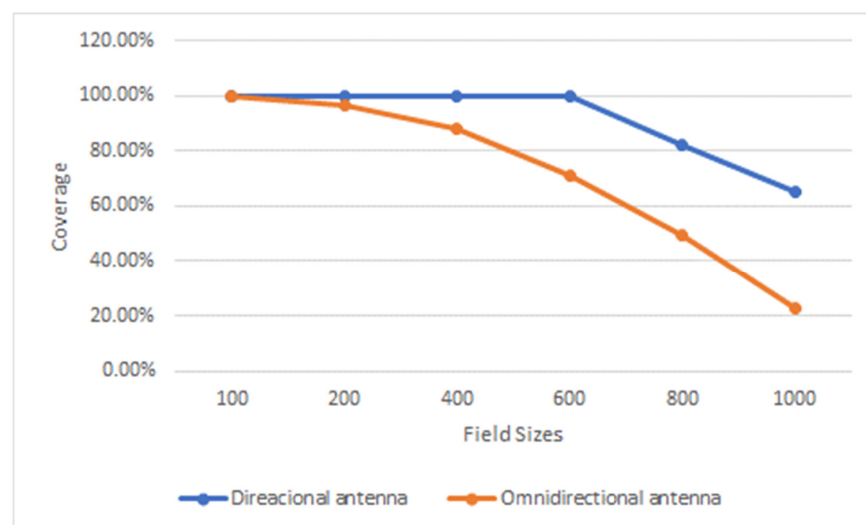


Figure 9. Experimental results (no. of BSs = 10; no. of UE = 1000).

4.5. Case Measurement

This research focuses on conducting automatic road inspections in the remote mountainous areas of Taoyuan, Taiwan. Road tests were performed using measurement equipment to record network transmission rates. The test locations are listed in Table 7 and primarily cover eight road sections in Fuxing District, Taoyuan City, with a total length of 33.2 km.

Table 7. Road inspection sections in remote mountainous areas.

Line	Road Name	Length (km)	Starting Point	Ending Point
1	Tao 113	8.1	0 + 000	8 k + 100
2	Tao 116	10	0 + 000	10 k + 000
3	Tao 112	4.3	0 + 000	4 k + 300
4	Tao 114	3.0	0 + 000	3 k + 000
5	Tao 115	3.2	0 + 000	3 k + 200
6	Tao 117	1.5	0 + 000	1 k + 500
7	Tao 118	2.1	0 + 000	2 k + 100
8	Tao 119	1.0	0 + 000	1 k + 000

The signal measurement results for this mountainous road area are shown in Figure 10, with the majority of signal transmission rates falling within the range of 5 Mbps to 20 Mbps, which ensures that IoT devices on road inspection vehicles can successfully transmit relevant road measurement data.

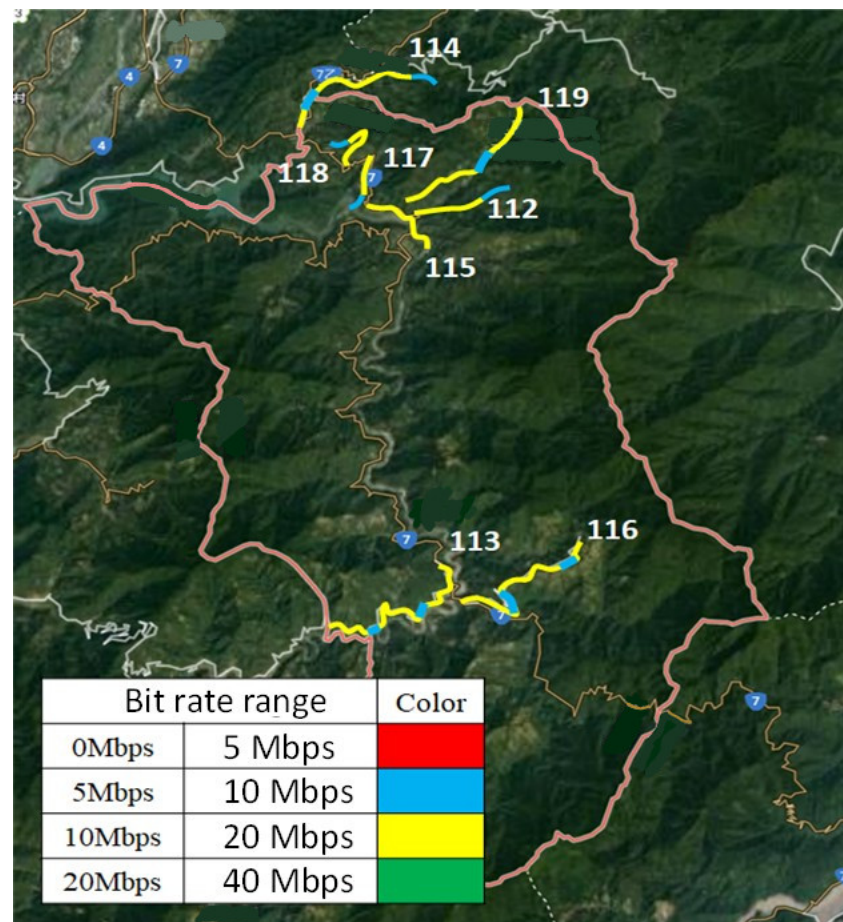


Figure 10. Network signal measurement results of the mountain roads.

4.6. Discussion

In this study, three simulation scenarios were analyzed. Unlike traditional omnidirectional antennas that can only modify signal coverage by adjusting base station power levels, this method introduces a novel approach. When compared with omnidirectional antennas, particularly in situations with higher user counts, such as 1200, the simulation results indicate an approximately 23.6% improvement in coverage rate. Moreover, with an increase in the number of base stations to 12, using omnidirectional antennas covered only 38.3% of the service area, while employing smart antennas enhanced the signal coverage rate to 78.1%. In larger testing areas, such as 1000 square meters, this method enhanced the field coverage rate by 42.8%.

The experimental results underscore the capability of this approach to adapt the radiation pattern of base stations to serve a larger number of users effectively in relatively spacious environments, even when the number of base stations is limited. This stands in contrast to conventional methods that primarily rely on adjusting base station power. This study presents a promising solution for enhancing signal coverage and capacity in scenarios with varying user densities and base station limitations.

5. Conclusions

In contrast to traditional omni-directional antennas that can only adjust signal coverage by varying base station power, the intelligent directional antennas used in this study offer the capability to not only adjust base station power, but also manipulate the five different antenna directions. This allows the user equipment (UE) within the antenna coverage area to receive stronger antenna gain signals. Additionally, the algorithm proposed in this research can determine the appropriate power settings for each base station and determine which antenna directions should be turned on or off within the entire network system. As a result, this approach can save energy consumption related to base station transmission power while simultaneously reducing UE interference.

Through experimentation, it was observed that coverage rates increased as the number of base stations (BS) increased and decreased as the test area expanded. Consequently, in practical deployments, it is recommended to increase the number of BS to counteract the coverage rate decrease caused by larger test areas.

In conclusion, the adoption of intelligent directional antennas with the proposed algorithm offers a promising solution to address signal interference and improve network coverage. By optimizing power settings and antenna configurations, the network can achieve higher coverage rates and better performance.

Author Contributions: Validation, L.-L.H.; Investigation, P.-Y.S.; Data curation, Y.-S.C.; Writing—original draft, M.-C.H.; Visualization, Y.-T.L. All authors have read and agreed to the published version of the manuscript.

Funding: This research received no external funding.

Data Availability Statement: The data are not publicly available due to privacy reasons.

Conflicts of Interest: The authors declare no conflict of interest.

References

1. Zhang, J.; Tu, G.; Liu, S.; Cai, Z. Audio Anti-Spoofing Based on Audio Feature Fusion. *Algorithms* **2023**, *16*, 317. [[CrossRef](#)]
2. Almeida, P.; Carvalho, V.; Simões, A. Reinforcement Learning Applied to AI Bots in First-Person Shooters: A Systematic Review. *Algorithms* **2023**, *16*, 323. [[CrossRef](#)]
3. Hong, T.; Sung, S.; Kang, H.; Hong, J. Advanced Real-Time Pollutant Monitoring Systems for Automatic Environmental Management of Construction Projects Focusing on Field Applicability. *ASCE J. Manag. Eng.* **2022**, *38*, 04021075. [[CrossRef](#)]
4. Lin, Y.C.; Cheung, W.F. Developing WSN/BIM-Based Environmental Monitoring Management System for Parking Garages in Smart Cities. *ASCE J. Manag. Eng.* **2020**, *36*, 04020012. [[CrossRef](#)]
5. Wang, X.; Liu, C.; Song, X.; Cui, X. Development of an Internet-of-Things-Based Technology System for Construction Safety Hazard Prevention. *ASCE J. Manag. Eng.* **2022**, *38*, 04022009. [[CrossRef](#)]

6. Yeo, C.J.; Yu, J.H.; Kang, Y. Quantifying the Effectiveness of IoT Technologies for Accident Prevention. *ASCE J. Manag. Eng.* **2020**, *36*, 04020054. [[CrossRef](#)]
7. Chandrasekhar, V.; Andrews, J.G. Uplink capacity and interference avoidance for two-tier femtocell networks. *IEEE Trans. Wirel. Commun.* **2009**, *8*, 3498–3509. [[CrossRef](#)]
8. Sundaresan, K.; Rangarajan, S. Efficient resource management in OFDMA femtocells. In Proceedings of the ACM International Symposium on Mobile Ad Hoc Networking and Computing, New Orleans, LA, USA, 18–21 May 2009.
9. Tseng, C.C.; Chen, K.C.; Su, C.W.; Lien, S.Y. Cognitive radio resource management for QoS guarantees in autonomous femtocell networks. In Proceedings of the IEEE International Conference Communication, Cape Town, South Africa, 23–27 May 2010.
10. Vlacheas, P.; Thomatos, E.; Tsagkaris, K.; Demestichas, P. Autonomic Downlink Inter-Cell Interference Coordination in LTE Self-Organizing Networks. In Proceedings of the International Conference on Network and Service Management, Paris, France, 24–28 October 2011.
11. Tao, C.; Koudouridis, G.P.; Qvarfordt, C.; Johansson, J.; Legg, P. Coverage and Capacity Optimization in E-UTRAN Based on Central Coordination and Distributed Gibbs Sampling. In Proceedings of the 2010 IEEE 71st Vehicular Technology Conference, Taipei, Taiwan, 16–19 May 2010.
12. Lee, H.C.; Oh, D.C.; Lee, Y.H. Mitigation of inter-femtocell interference with adaptive fractional frequency reuse. In Proceedings of the IEEE International Conference Communication, Cape Town, South Africa, 23–27 May 2010.
13. Mérida-Calvo, L.; Feliu-Talegón, D.; Feliu-Battle, V. Improving the Detection of the Contact Point in Active Sensing Antennae by Processing Combined Static and Dynamic Information. *Sensors* **2021**, *21*, 1808. [[CrossRef](#)] [[PubMed](#)]
14. Lee, C.-Y.; Kim, J.-H. Active Flutter Suppression of Smart-Skin Antenna Structures with Piezoelectric Sensors and Actuators. *Aerospace* **2021**, *8*, 257. [[CrossRef](#)]
15. Yanyun, C.; Alexis, H.; Hui, X.; Xingxiu, Y. Coverage and Capacity Optimization for 4G LTE Networks Using Differential Evolution. In Proceedings of the 2018 5th IEEE International Conference on Cloud Computing and Intelligence Systems (CCIS), Nanjing, China, 23–25 November 2018; pp. 640–645.
16. Zuiddam, J. The Asymptotic Spectrum of Graphs and the Shannon Capacity. *Combinatorica* **2019**, *39*, 1173–1184. [[CrossRef](#)]
17. Maharazu, M.; Hanapi, Z.M.; Alrashah, M.A. Energy and Spectral Efficiency Balancing Algorithm for Energy Saving in LTE Downlinks. *Symmetry* **2021**, *13*, 211. [[CrossRef](#)]

Disclaimer/Publisher’s Note: The statements, opinions and data contained in all publications are solely those of the individual author(s) and contributor(s) and not of MDPI and/or the editor(s). MDPI and/or the editor(s) disclaim responsibility for any injury to people or property resulting from any ideas, methods, instructions or products referred to in the content.